Available online at www.sciencedirect.com

ScienceDirect

International Journal of Solids and Structures 44 (2007) 8313–8334

INTERNATIONAL JOURNAL OF SOLIDS AND STRUCTURES

www.elsevier.com/locate/ijsolstr

On the determination of the Young's modulus of thin films using indentation tests

J.M. Antunes [a,b,*], J.V. Fernandes [a], N.A. Sakharova [a], M.C. Oliveira [a], L.F. Menezes [a]

[a] *CEMUC – Department of Mechanical Engineering, University of Coimbra, Rua Luís Reis Santos, Pinhal de Marrocos, 3030-788 Coimbra, Portugal*

[b] *Escola Superior de Tecnologia de Abrantes, Instituto Politécnico de Tomar, Rua 17 de Agosto de 1808, 2200 Abrantes, Portugal*

Received 17 April 2007; received in revised form 29 May 2007; accepted 15 June 2007
Available online 21 June 2007

Abstract

The main difficulty with the characterization of thin coatings using depth-sensing indentation tests is related to the determination of the contributions of the substrate and the film to the measured properties. In this study, three-dimensional numerical simulations of the Vickers hardness test are used in order to examine the influence of the elastic and plastic properties of the substrate and the film on the composite's Young's modulus results. The hardness of the film is equal to or higher than the substrate hardness. A study of the stress distributions and the indentation geometry of composites, film/substrate, was performed, taking into account the relative mechanical properties of the film and substrate. In addition, stress evolution during indentation was studied, in order to quantify the critical indentation depth under which the substrate is not elastically deformed. The accurate evaluation of the Young's modulus of the films using weight functions is also examined: some of these have previously been proposed and one was introduced for this study. Two different fitting procedures were used to compare the results obtained from eight fictive film/substrate combinations using six weight functions. The first procedure, commonly used, considers the substrate's modulus as a known parameter in the fitting process. In the second, the film and the substrate's modulus are considered as unknown variables that are calculated simultaneously during the fitting process. The validity of the conclusions obtained using the fictive materials was checked by applying the weight functions to four real composites.

Keywords: Thin films; Vickers indentation; Numerical simulation

1. Introduction

One of the most important mechanical properties in surface characterization is the Young's modulus. The principal advantage in the use of the depth-sensitive indentation technique for the Young's modulus evaluation

* Corresponding author. Address: CEMUC – Department of Mechanical Engineering, University of Coimbra, Rua Luís Reis Santos, Pinhal de Marrocos, 3030-788 Coimbra, Portugal. Tel.: +351 239 790700; fax: +351 239 790701.
E-mail address: jorge.antunes@dem.uc.pt (J.M. Antunes).

0020-7683/$ - see front matter
doi:10.1016/j.ijsolstr.2007.06.015

is that it has no special requirements for the sample size and geometry. However, in hardness tests on thin films, as the indentation depth increases, not only does the film deform but the substrate also often presents elastic and plastic deformation. In this way, the mechanical property evaluation of the composite is a complex function of the film and substrate's mechanical properties, which depends on the maximum applied load (e.g., Doerner et al., 1986; Fabes et al., 1992; Page and Hainsworth, 1993; Chechenin et al., 1995; Tsui et al., 1999a,b; Saha and Nix, 2002). The obvious solution for the correct mechanical property evaluation of thin films requires the use of low loads, in order to obtain only the film's contribution. In order to measure the Young's modulus of the film a commonly used rule is to limit the maximum indentation depth to less than 10% of the film's thickness (Pharr and Oliver, 1992). However, this procedure cannot be applied to very thin films, for which very low indention depths are needed. In this case, strong scatter in the data of hardness tests can appear, due to the roughness of the sample surface, for example.

In this context, alternative methods for the Young's modulus evaluation of thin films that consider the substrate's contribution must be developed and improved, i.e. complete knowledge of the substrate's effects on the results of the mechanical properties of the films is needed. Several previous experimental and theoretical studies have been done to analyse the problem of extracting the Young's modulus of thin films considering substrate influence (Burnett and Rickerby, 1987; Joslin and Oliver, 1990; Menčík et al., 1997; Korsunsky et al., 1998; Tsui and Pharr, 1999). Also, numerical simulation has been used as an auxiliary tool to acquire better understanding of the indentation process (King, 1987; Bhattacharya and Nix, 1988; Sun et al., 1995; Chen and Vlassak, 2001; Antunes et al., 2004).

In this study, the authors make use of the finite element method to simulate the Vickers indentation tests of the film/substrate of different systems. Results of 3D-numerical simulations of different composites were used to study stress distributions. The problem of evaluating the film's Young's modulus is analysed using six different weight functions applied to several fictitious and real composite materials, with the purpose of improving the methodology and approaches to Young's modulus evaluation of thin films.

2. Theoretical analysis

Using depth-sensing indentation tests, the Young's modulus is determined from (e.g., Sneddon, 1965; Oliver and Pharr, 1992):

$$E^{\mathrm{SI}} = \frac{1}{\beta}\frac{\sqrt{\pi}}{2}\frac{1}{\sqrt{A}}\frac{1}{C}, \tag{1}$$

where β is a correction factor that considers the indenter geometry. A is the contact area of the indentation at maximum load and C is the compliance. E^{SI} is the "specimen + indenter" modulus. The specimen's elastic modulus E, that depends on the film and substrate's elastic modulus (E_{f} and E_{s}, respectively) is determined using the definition:

$$\frac{1}{E^{\mathrm{SI}}} = \frac{1}{E^*} + \frac{1}{E_{\mathrm{i}}^*}, \tag{2}$$

with

$$E^* = E/(1-\nu^2) \text{ and } E_{\mathrm{i}}^* = E_{\mathrm{i}}/(1-\nu_{\mathrm{i}}^2), \tag{3}$$

where E^* and E_{i}^* are the reduced modulus and ν and ν_{i} are the Poisson's ratios of the specimen and of the indenter, respectively.

In the case of elastically homogeneous composites, film and substrate have the same reduced Young's modulus, i.e., $E_{\mathrm{f}}^* = E_{\mathrm{s}}^*$ and E^* represents the value of the reduced elastic modulus of the specimen: $E^* = E_{\mathrm{f}}^* = E_{\mathrm{s}}^*$. If the film and substrate are not elastically homogeneous, the reduced modulus evaluated with Eqs. (2) and (3) does not correspond only to the film, especially if the film is very thin and/or the ratio between the Young's modulus of the film and substrate is very different from 1.

When the reduced Young's modulus of the film, E_{f}^*, and the substrate, E_{s}^*, differ the evaluated reduced indentation modulus of the specimen, E^*, depends on the indentation depth. With an increase in the indentation depth, the Young's modulus, E^*, changes gradually from the value of the film to the one of the substrate.

As consequence, for the maximum indentation depths normally used in experimental tests, the evaluated Young's modulus depends on the substrate's presence.

Weight functions have been used for the evaluation of reduced Young's moduli of thin coatings, E_f^*. These functions depend on the value of E_s^* and on the ratio h/t (where h and t are the contact indentation depths at the maximum load and the film thickness, respectively). The easiest and most commonly used way to determine the value of E_f^*, by fitting the experimental results and applying a weight function, is to already know the value of E_s^* (e.g., Doerner et al., 1986; Menčík et al., 1997; Saha and Nix, 2002).

Exponential type functions can be used to fit the result of the composite Young's modulus evaluated at different maximum indentation depths. Below, some typical exponential functions are described. Menčík et al. (1997) proposed the following equation:

$$\frac{\left|E^* - E_s^*\right|}{\left|E_f^* - E_s^*\right|} = e^{\left(-\alpha_1 \frac{h}{t}\right)}, \tag{4}$$

where α_1 is a constant that is determined in the fitting procedure. Fig. 1(a) shows a representation of this function for both cases, $E_f^* > E_s^*$ and $E_f^* < E_s^*$.

Eq. (4) can be developed in a linear form: $y = A + B(h/t)$, where $y = \ln|E^* - E_s^*|$. The constants, $A = \ln|E_f^* - E_s^*|$ and $B = -\alpha_1$, can be obtained using a least squares method. Knowing the value of E_s^*, the reduced film Young's modulus, E_f^*, can be calculated as follows: $E_f^* = E_s^* + ke^A$, where $k = 1$ if $E_f > E_s$, and $k = -1$ if $E_f < E_s$.

Another proposed weight function is the reciprocal of the exponential function defined as (Menčík et al., 1997):

$$\frac{\left|1/E^* - 1/E_s^*\right|}{\left|1/E_f^* - 1/E_s^*\right|} = e^{\left(-\alpha_2 \frac{h}{t}\right)}, \tag{5}$$

where α_2 is a constant that is determined in the fitting procedure. This function can also be used for both cases, $E_f^* > E_s^*$ and $E_f^* < E_s^*$ as is shown in Fig. 1(a). The procedure for determining the reduced film Young's modulus can be similar to the one used for the exponential function (Eq. (4)).

Doerner and Nix (1986) propose also an exponential function of the same type as Eq. (5) but changing h/t by t/h:

$$\frac{\left|1/E^* - 1/E_f^*\right|}{\left|1/E_f^* - 1/E_s^*\right|} = e^{\left(-\alpha_3 \frac{t}{h}\right)}, \tag{6}$$

where α_3 is a constant that is determined in the fitting procedure. The representation of this function is shown in Fig. 1(b), for $E_f^* > E_s^*$ and $E_f^* < E_s^*$. Eq. (6) cannot be transformed so that the determination of the unknown constants α_3 and E_f^*, from a group of composite Young's modulus values obtained at different

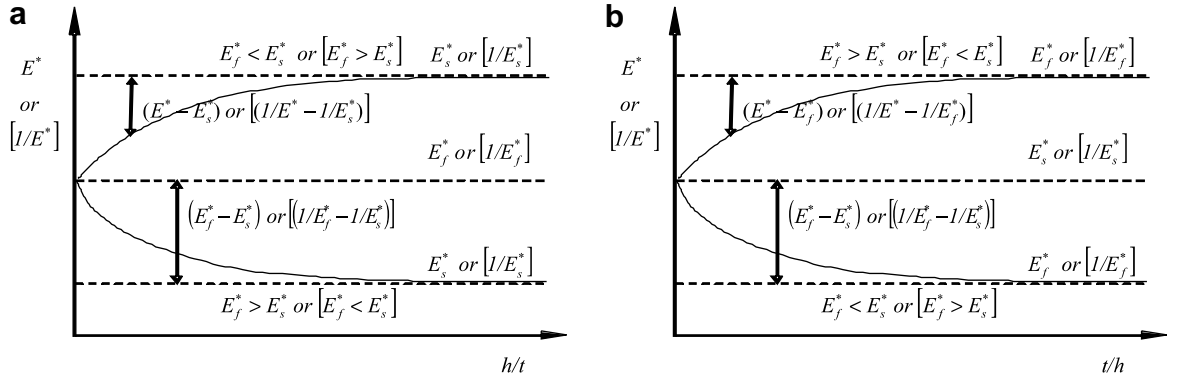

Fig. 1. Schematic representation of the four exponential functions for the cases $E_f^* > E_s^*$ and $E_f^* < E_s^*$. (a) Exponential (Eq. (4)) and Reciprocal of exponential (Eq. (5)). (b) Doerner and Nix (Eqs. (6) and (7)).

indentation depths, becomes a more difficult task. In this case an optimization procedure is used for the determination of the optimum combination of α_3, E_f^* (Menčík et al., 1997).

Although, not previously proposed in the literature to our knowledge, a fourth exponential function can be used for cover all possibilities of exponential functions. This equation is expressed by:

$$\frac{\left|E^* - E_f^*\right|}{\left|E_f^* - E_s^*\right|} = e^{\left(-\alpha_4 \frac{t}{h}\right)}, \tag{7}$$

where α_4 is a constant that is determined in the fitting procedure. This equation can also be used in both cases, $E_f^* > E_s^*$ and $E_f^* < E_s^*$, as is shown in Fig. 1(b). The optimization procedure suggested for Eq. (6), can be used for the determination of the optimum combination of α_4 and E_f^*.

Gao et al. (1992), also proposed a function for the determination of the reduced film's Young's modulus. The function, based on the analytical solution of the contact of a rigid cylindrical indenter with an elastic layered body, has the form:

$$\frac{\left(E^* - E_s^*\right)}{\left(E_f^* - E_s^*\right)} = \Phi, \tag{8}$$

where Φ is the Gao's weight function, given by:

$$\Phi = \frac{2}{\pi}\arctan\left(\frac{a}{t}\right) + \frac{1}{2\pi(1-\nu)}\left[(1-2\nu)\frac{a}{t}\ln\left(1+\left(\frac{a}{t}\right)^2\right) - \frac{\frac{a}{t}}{1+\left(\frac{a}{t}\right)^2}\right], \tag{9}$$

where a is the contact radius of a cylindrical flat punch indentation at the maximum load. A relationship can be established between a and h, considering for example that the projected contact area of the pyramidal indenter is equal to the area of the cylindrical flat punch; in the case of a Vickers indenter this leads to: $a = h\sqrt{24.5/\pi}$. The typical procedure for extracting the Young's modulus of the film uses the composite Young's modulus values obtained at different indentations depths. Eq. (8) transformed corresponds to a straight line that crosses the origin of the coordinate system ($y = Bx$), where $y = E^* - E_s^*, B$ is $E_f^* - E_s^*$ and x is the result of Eq. (9) for the different indentations depths. The constant B is calculated using a least square method. The reduced Young's modulus of the film is then obtained by $E_f^* = E_s^* + B$. This equation can be used for both cases: $E_f^* > E_s^*$ and $E_f^* < E_s^*$.

3. Numerical simulation and materials

The numerical simulations of the hardness test were performed using the HAFILM home code, which was developed to simulate this type of test. This code simulates hardness tests with any type of indenter geometry, and takes into account the friction between the indenter and the deformable body. It considers the hardness test to be a quasi-static process that produces large deformations and makes use of a fully implicit algorithm of Newton–Raphson type to solve in a single iteration loop both non-linearities: the evolution in deformation and the contact between the indenter and the deformable body (Menezes and Teodosiu, 2000; Antunes et al., 2006).

The Vickers indenter used in the numerical simulations considers the most common defect of the tip, usually designated as *offset*. The tip of the indenter presents a rectangular shape with an area of 0.0288 μm^2 (Antunes et al., 2002, 2006). The indenter geometry is described by Bézier surfaces, which allow a fine description of the tip.

For the description of the test sample, that corresponds to a cylinder with a radius and height of 40 μm, the HAFILM code makes use of a finite element mesh composed of three-linear eight-node isoparametric hexahedrons associated with a selective reduced integration technique (Menezes and Teodosiu, 2000). In this study, the finite element mesh was composed of 7992 elements. The coating thickness is 0.5 μm and is composed of nine layers of elements. In addition, to test the influence of the film's thickness on the Young's modulus results another finite element mesh was considered with a coating of 0.165 μm (3 layers of elements in the coating). In the meshes, the size of the finite elements in the indentation region is about 0.055 μm. This mesh refinement was chosen in order to guarantee a high degree of accuracy in the indentation contact area (Antunes et al.,

2006, 2007). Fig. 2 presents a detail of the indentation region of the finite element mesh (coating thickness of 0.5 μm) at the beginning of the simulation. Due to the symmetry in the planes $X = 0$ and $Z = 0$ (Fig. 2), only a fourth of the sample was used in the numerical simulations. The friction between the indenter and the sample was considered to be a coefficient equal to 0.16 (Antunes et al., 2006, 2007).

Three-dimensional numerical simulations of the Vickers hardness test were performed on 10 fictitious composites, with a film thickness of 0.5 μm, using different maximum indentation depths ($h_{max} = 0.05$, 0.06, 0.1, 0.15, 0.25, 0.35, 0.45, 0.55 and 0.65 μm). In two particular cases, a film thickness equal to 0.165 μm was also considered in the numerical simulations, for the maximum indentations depths of 0.03, 0.08, 0.16 and 0.21 μm.

The composite Young's modulus, E, was evaluated with Eq. (1); where the correction factor, β, was considered equal to 1.05 for the Vickers indenter (Antunes et al., 2006, 2007). The compliance, C, was evaluated from the slope of the upper portion of the unloading curve, using the equation (70% of unloading curve was fitted) (Antunes et al., 2006):

$$P = P_0 + T(h - h_0)^q, \tag{10}$$

where P_0 is the lower load considered in the fit of the unloading curve, corresponding to indentation depth h_0; T and q are the fitted constants. The load–unloading curves were corrected with the area function of the Vickers indenter. For the evaluation of the indentation contact area, A, the calculations used the contour of the nodes in the finite element mesh in contact with the indenter at the maximum load (Antunes et al., 2006).

The values of the Young's modulus of the materials studied are between 100 and 600 GPa, for the film, and between 100 and 400 GPa, for the substrate. Six cases of the ratio E_f/E_s were studied: $E_f/E_s = 0.25$, 0.5, 1, 2, 3 and 4. For the case of $E_f/E_s = 3$, two possibilities were considered: $E_f/E_s = 300/100$ and 600/200. A Poisson ratio of 0.3 was used for all the materials (films and substrates). Two values of the ratio between the yield stress of the film and substrate, σ_f/σ_s (1 and 2), were also tested.

The plastic behaviour of the materials used in the numerical simulations was modulated considering that the relationship between the stress, σ, and plastic strain, ε, of the film and the substrate are described by the Swift law: $\sigma = k(\varepsilon + \varepsilon_0)^n$, where k, ε_0 and n are material constants (the material yield stress is: $\sigma_y = k\varepsilon_0^n$). Table 1 summarizes the mechanical properties of the composites used in the numerical simulations.

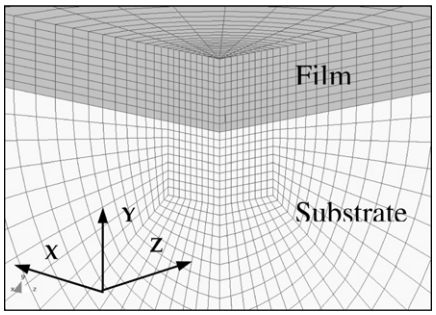

Fig. 2. Detail of the indentation region of the finite element mesh with a 0.5 μm coating thickness, used in the numerical simulations.

Table 1
Mechanical properties of the simulated composites

Composites	σ_f (GPa)	σ_s (GPa)	n	E_f (GPa)	E_s (GPa)	ε_0	ν	σ_f/σ_s	E_f/E_s
C1	2	2	0.01	400	100	0.005	0.3	1	4
C2	2			300				1	3
C3	2			600	200			1	3
C4	4			400				2	2
C5	2			400				1	2
C6	4			200				2	1
C7	2			200				1	1
C8	4			100				2	0.5
C9	2			100				1	0.5
C10	2			100	400			1	0.25

4. Results and discussion

4.1. Strain and stress distributions, and indentation geometry

The development of stress in the indentation region was studied to acquire a better understanding of the influence of the substrate and the film on the determined mechanical properties of the composite. In fact, there are important aspects related to the development of stress under indentation during hardness testing. For instance, it is important to know the critical indentation depth, under which the substrate is not elastically deformed and then does not have any influence on the measured mechanical proprieties. The accuracy of the contact area values and, consequently, of the Young's modulus, depends on the geometry of the indentation. In the case of soft bulk materials, for example, the presence of strong pile-up on the indentation surface promotes the underestimation of the contact area, and the Young's modulus is overvalued, mainly for materials in which h_f/h_{max} approaches 1. As discussed below, the indentation geometry obtained for the composites depends not only on the relationship between the mechanical properties of the film and the substrate but also on the maximum indentation depth.

In order to clarify the influence of the ratio E_f/E_s and of the maximum indentation depth on the composites' behaviour, the study of the equivalent stress distribution of the composites with $E_f > E_s$ and $E_f < E_s$ was performed for the group of composites with $\sigma_f/\sigma_s = 1$. Figs. 3 and 4 present the von Mises equivalent stress dis-

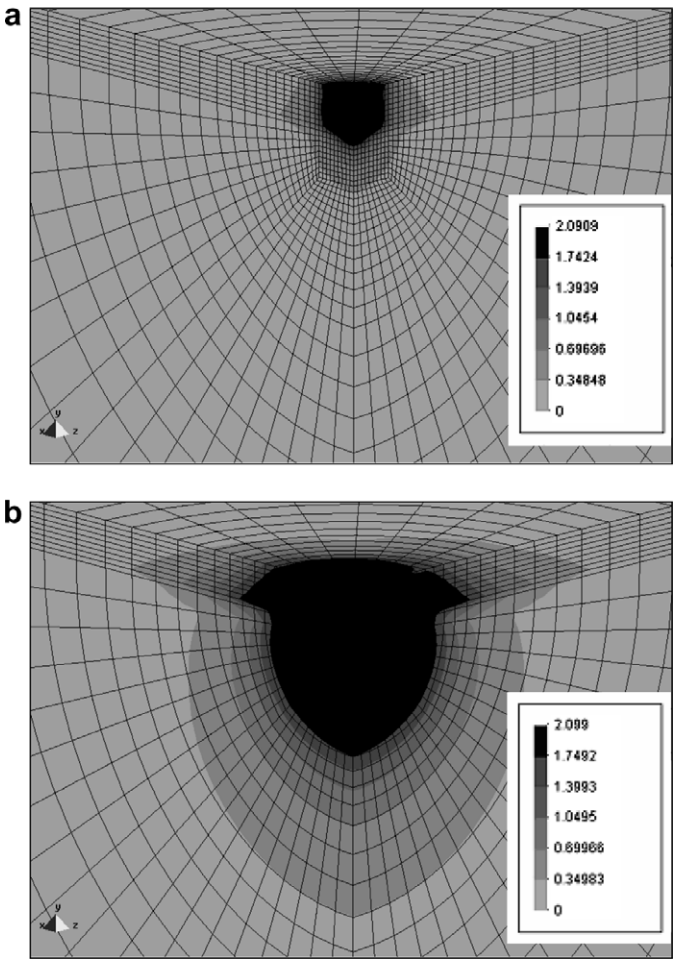

Fig. 3. Von Mises equivalent stress distribution (GPa) obtained at the maximum load in the numerical simulations of the composite C1. (a) $h_{max}/t = 0.1$ μm. (b) $h_{max}/t = 0.5$ μm.

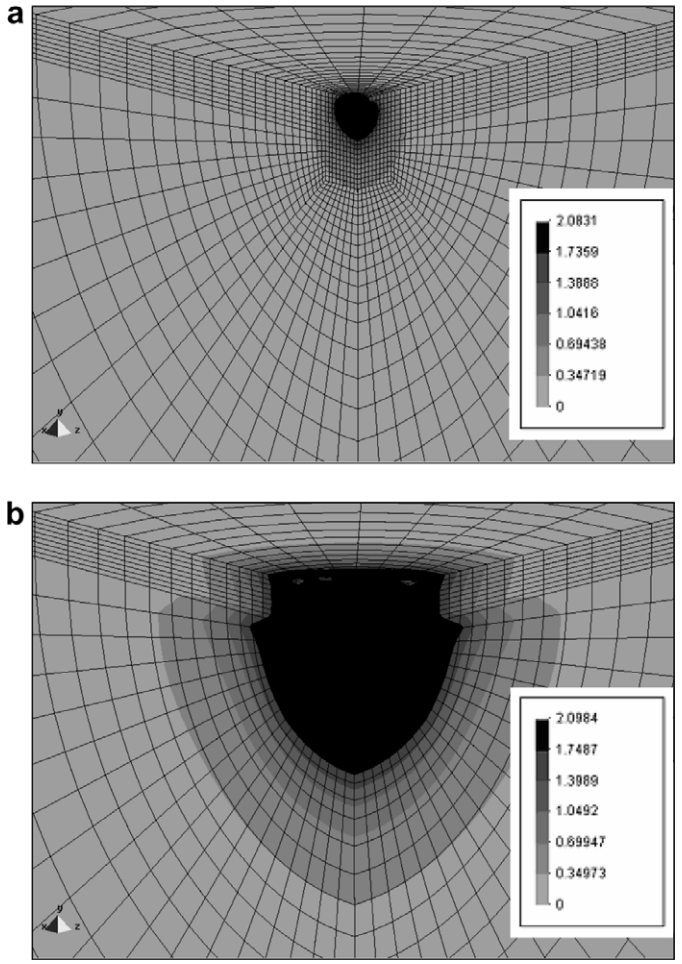

Fig. 4. Von Mises equivalent stress distribution (GPa) obtained at the maximum load in the numerical simulations of the composite C10. (a) $h_{max}/t = 0.1$ μm. (b) $h_{max}/t = 0.5$ μm.

tribution at the maximum relative indentation depths, h_{max}/t, 0.1 and 0.5, respectively for composites C1 and C10 (E_f/E_s equal to 4 and 0.25, respectively). The equivalent stress distributions obtained with the C1 (Fig. 3) and C10 (Fig. 4) composites show a region with high values under the indentation region, that increase as maximum indentation depth increases. The size of the elastically deformed region (equivalent stress higher than zero) at the surface relative to the size of the same region at the interface substrate/film is higher than 1, for the case of composite C1 ($E_f/E_s = 4$), and lower than 1, for composite C10 ($E_f/E_s = 0.25$). This suggests that the relative contribution of the film to the composite's behaviour must be higher in the case of composite C1, than that observed for composite C10. For composite C1, the depth of the elastically deformed region, measured from the surface of the sample, increases from 3.3 to 7.2 μm, as the maximum indentation depth increases from 0.1 to 0.5 μm (Fig. 3). On the other hand, composite C10 ($E_f/E_s = 0.25$) initially exhibits a larger influence of the substrate (Fig. 4). For a maximum relative indentation depth, h_{max}/t, of 0.1, the depth of the elastically deformed region of composite C10 is lower (1.8 μm) than the one obtained for composite C1 (Fig. 4). However, as the maximum indentation depth increases the extension of the region with equivalent stress higher than zero becomes identical to the one obtained for composite C1 (7.5 μm).

A study was performed to evaluate the limit of the penetration depth for which the substrate starts to deform elastically. The results have shown that when the penetration depth is greater than 0.001 μm, the substrate region shows an equivalent stress level higher than zero. This means that the substrate deforms elastically from the beginning of the indentation test. This is probably associated with the size of the offset of the

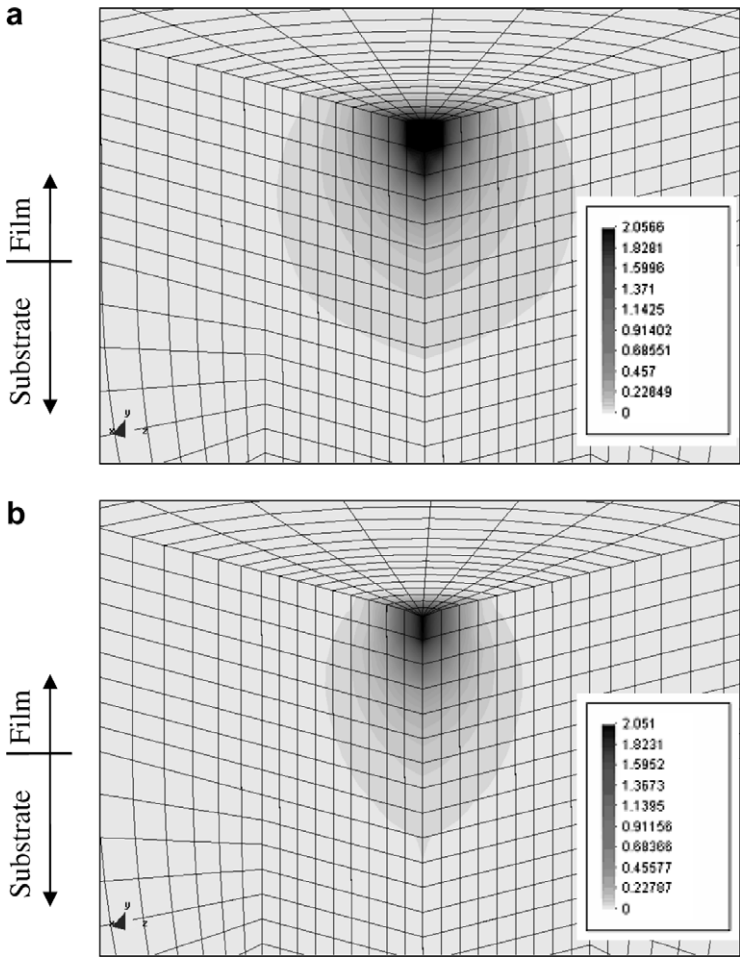

Fig. 5. Von Mises equivalent stress distribution (GPa) obtained in the numerical simulations. (a) Composite C1. (b) Composite C10.

indenter, which has an area of 0.0288 μm^2, close to that experimentally observed in Vickers indenters. To confirm this hypothesis, new simulations were performed with an almost perfect indenter which had an offset area equal to 0.0032 μm^2. The results of these simulations for composites C1 and C10 are shown in Fig. 5. It is clear from the results that, even for this indenter, the indentation depths for which the elastic deformation starts in the substrate are not significant: 0.005 μm for composite C1, and 0.006 μm for composite C10. Consequently, it can be concluded that even for a relatively high thickness of film (0.5 μm) signs of the elastic deformation in the substrate appear so early that, in typical indentation tests, the measured Young's modulus results are not only those of the film.

In order to understand the influence of the substrate on the determination of the Young's modulus of the film, a study was undertaken concerning the "*error*" made in the determination of the film's Young's modulus when this is considered equal to the composite Young's modulus, obtained at a given relative penetration depth (h/t). Therefore, the "*error*" is equal to $(E_f - E)/E_f$, where E_f and E are the Young's moduli of film and composite, respectively. Fig. 6 shows the $(E_f - E)/E_f$ results versus the E_f/E_s ratio, for a relative penetration depth (h/t) of 5% (set of composites for which σ_f/σ_s is equal to 1). The $(E_f - E)/E_f$ increases when the E_f/E_s ratio moves away from 1. Moreover, for the composites with E_f/E_s ratios of 0.25 and 0.5, the $(E_f - E)/E_f$ values are close to −15.2% and −6.5%; for the remaining composites, this value is of about 12.5%, 16.7% and 21.3% for E_f/E_s ratios of 2, 3 and 4, respectively. These results show that when making use of a low relative penetration depth to determine the Young's modulus without using a weight function, relatively high errors can occur, depending on the ratio E_f/E_s. This fact suggests that the use of higher penetration depths associated

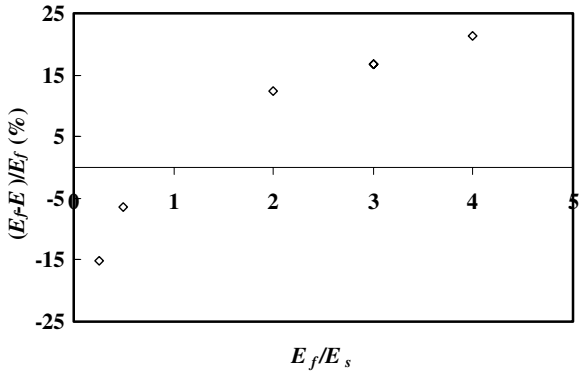

Fig. 6. Evolution of $(E_f - E)/E_f$ as a function of the ratio E_f/E_s, for a relative penetration depth (h/t) of 5%.

with an accurate model (weight function) may be a better way of obtaining accurate results of the film's Young's modulus than the use of a single measurement at low indentation depths.

The stress distributions of (σ_{xx} and σ_{yy}, according to the axes shown in Fig. 2) and the corresponding indentation geometry, were also evaluated to complement the analysis of the composites' behaviour. The results presented in Fig. 7 correspond to these stress components' distribution for composites C4 and C5, obtained at the surface of the indentation, at a maximum indentation depth of 0.15 μm. The indentation profiles

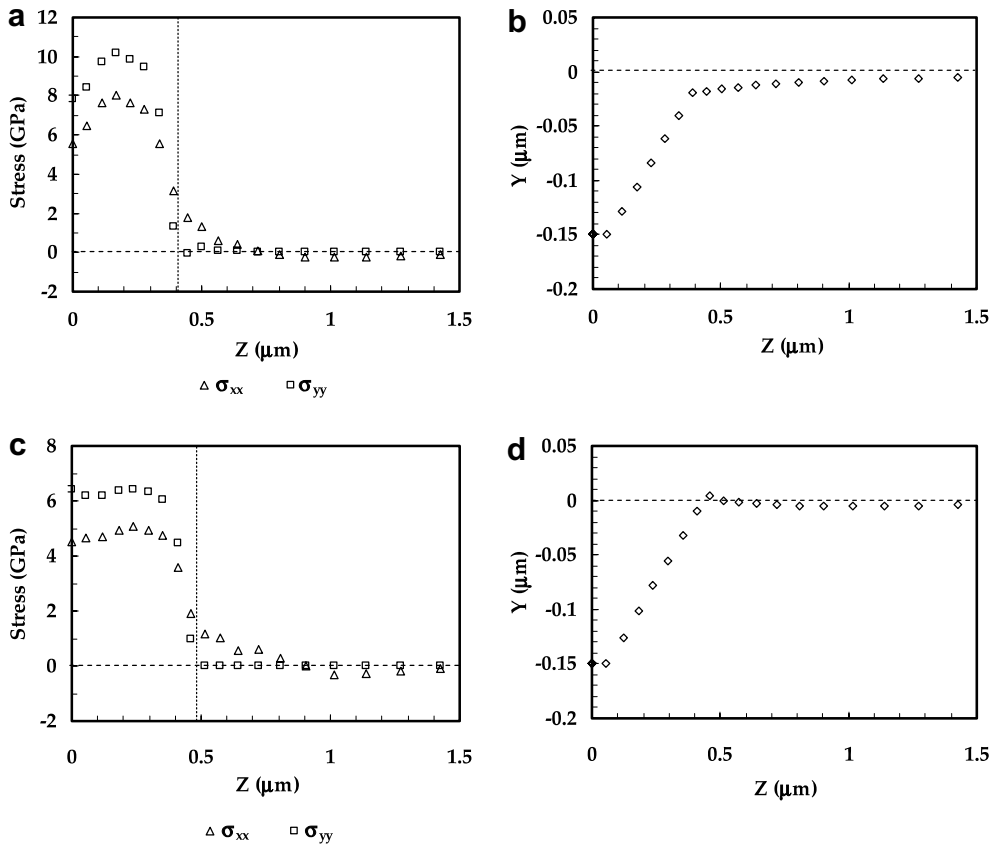

Fig. 7. Stress distributions of σ_{xx} and σ_{yy} and indentation profiles obtained at the maximum load ($h_{max} = 0.15$ μm) in the numerical simulations of the composites with ratio $E_f/E_s = 2$ (C4 and C5). (a) and (b) $\sigma_f/\sigma_s = 2$. (c) and (d) $\sigma_f/\sigma_s = 1$.

obtained at this indentation depth are also shown. The stress distributions presented in Fig. 7(a) and (c) show that the regions with compressive stresses correspond to the region in contact with the indenter (the vertical dashed line in Fig. 7(a) and (c) represents the contact boundary). The stress distributions obtained for the remaining composites are similar to those shown in Fig. 7. The evolution of indentation geometry (from sink-in to pile-up) is different when the σ_f/σ_s ratios have a value of 1 or 2, as exemplified in Fig. 7(b) and (d), for $E_f/E_s = 2$.

The evolution of indentation surface geometry with maximum indentation depth was also analysed considering the position (height) of the higher contact point, Δh, in relation to the initial surface plane of the sample. The contact points correspond to the nodes of the finite element mesh in contact with the indenter surface. Fig. 8 presents the definition of the height of the contact point, Δh, considering the two indentation surface geometries, pile-up ($\Delta h > 0$) and sink-in ($\Delta h < 0$), respectively. Fig. 9 shows the results of the height of the contact point, Δh, as a function of the maximum indentation depth, for the composites that the ratio σ_f/σ_s is 1 and the Young's modulus ratios E_f/E_s are 4 (composite C1), 3 (C2), 2 (C3), 2 (C5), 0.5 (C9) and 0.25 (C10). The continuous lines represent the evolution of the contact point height, Δh, in the case where the films and the substrates are tested as bulk materials. The above evolutions were considered linear taking into account those

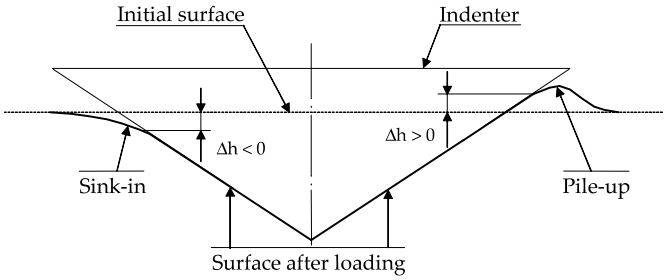

Fig. 8. Height of the limit contact point, Δh, in relation to the initial surface.

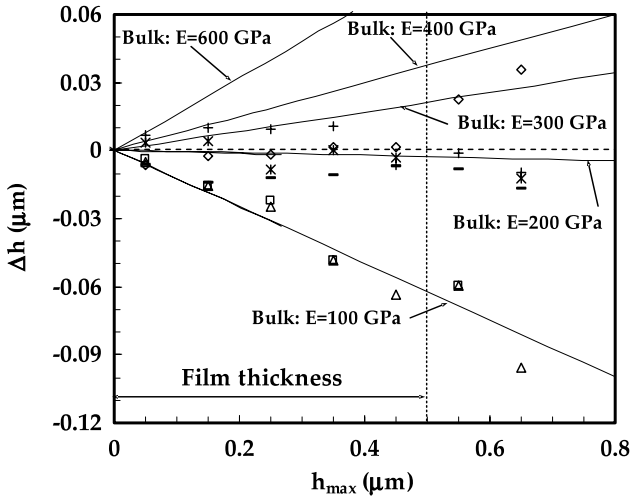

	□ C1	△ C2	+ C3	* C5	– C9	◇ C10
E_f (GPa)	400	300	400	600	100	100
E_s GPa)	100	100	200	200	200	400
E_f/E_s	4	3	2	2	0.5	0.25

Fig. 9. Evolution of the height of the limit contact point, Δh, versus the maximum indentation depth for the composites with ratio σ_f/σ_s equal to 1.

observed in previous studies about the indentation of different bulk materials (see e.g., Antunes et al., 2007). Fig. 9 shows that the evolution of the indentation profiles with the indentation depth obtained for the composites C1 and C2 are close to the ones where the bulk material is similar to the substrate. On the other hand, composites C3 and C5 exhibit pile-up formation at low indentation depths (as bulk materials with mechanical properties equal to the films of the composites C3 and C5). However, as indentation depth increases, the surface profile approaches that of the bulk material similar to the substrate (low sink-in). In the case of composites C9 and C10 (for which sink-in is observed when the films are tested as bulk materials), initially the indentation profiles exhibit sink-in that decreases with the increase of the indentation depth. Moreover, in the case of composite C10, material pile-up formation appears for values of the indentation depth close to the film thickness (the bulk material similar to the substrate shows pile-up). In conclusion, for the composites with ratio σ_f/σ_s equal to 1, the indentation surface geometry evolves with indentation depth from the typical behaviour of the film to the typical behaviour of the substrate.

A similar study was also performed for the composites where the σ_f/σ_s ratio is 2 and E_f/E_s is 2, 1 and 0.5 (composites C4, C6 and C8, respectively). The results are shown in Fig. 10. For these composites the indentation profiles always exhibit sink-in, in contrast to similar composites where the σ_f/σ_s ratio is 1 (composites C5, C7 and C9, respectively). The results of composites C5, C7 and C9 are also shown in Fig. 10, for comparison. In conclusion, the composite's indentation geometry depends on the indentation depth: in other words the evolution of Δh versus h_{max} is non-linear; the opposite of that observed for bulk materials.

Previous studies of bulk materials have shown that accurate evaluation of the indentation contact area depends on the presence of pile-up or sink-in (see e.g., Bolshakov et al., 1997; Antunes et al., 2006). This indentation geometry appear for low values of the ratio (H/E) between the hardness, H, and the Young's modulus, E, (equivalent to values of the ratio between the residual and maximum indentation depth, h_f/h_{max}, close to 1) in the case of materials with low work-hardening (Bolshakov et al., 1997; Antunes et al., 2006). In this case, the indentation contact area is underestimated and consequently the Young's modulus is overestimated. In the current study, where the work-hardening value $n = 0.01$ was used, the values of h_f/h_{max} for which pile-up occurs are higher than 0.86, in case of bulk materials. This result had already been obtained in a detailed

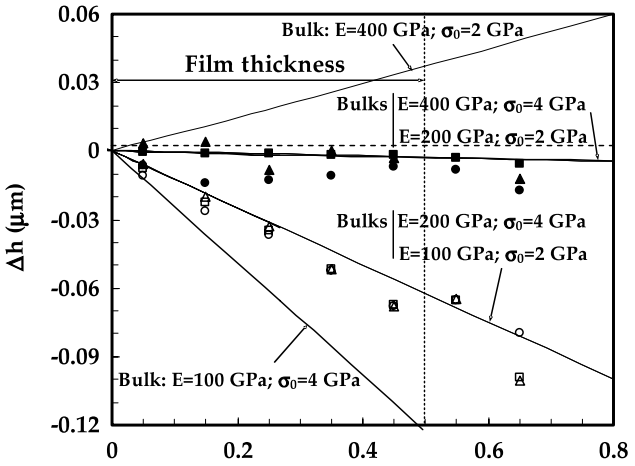

σ_f/σ_s=2	△ C4	□ C6	○ C8
σ_f/σ_s=1	▲ C5	■ C7	● C9
E_f (GPa)	400	200	100
E_s (GPa)	200	200	200
E_f/E_s	2	1	0.5

Fig. 10. Evolution of the height of the limit contact point, Δh, versus the maximum indentation depth for the composites with ratio σ_f/σ_s equal to 2 and 1, and ratio E_f/E_s equal to 2, 1 and 0.5.

study using the current finite element code and simulation conditions (Antunes et al., 2006). Qualitatively similar results (h_f/h_{max} close to 0.82, for $n = 0$) were obtained by Bolshakov et al. (1997), for a conical indenter without friction between the sample and the indenter in a 2D finite element simulation.

4.2. Young's modulus of the film

In this section, we will analyse the evolution of the Young's modulus of the composite, E (and $1/E$) versus the normalized penetration depth h/t (and t/h), in order to check the performance of the models described above, to accurately determine the film's Young's modulus. In addition, a new model based on the Gao et al. (1992) function is proposed and compared to the previous models. In the first stage, the numerical results of the fictitious composites are used. Afterwards, the experimental results obtained from four real composites are considered.

4.2.1. Fictitious composites

Fig. 11 shows the results of the Young's modulus obtained by numerical simulations of the composites C6 and C7 (Table 1), at different maximum indentation depths. These composites have the same value of Young's modulus for the film and for the substrate (E_f/E_s equal to 1) and two different ratios between the yield stresses of the film and the substrate (composite C6: σ_f/σ_s equal to 2; composite C7: σ_f/σ_s equal to 1). Fig. 11 shows that the composite Young's modulus results are accurately determined for both composites. This fact indicates that the use of correction factor β (equal to 1.05 in Eq. (1)), previously proposed for bulk materials (Antunes et al., 2006), remains appropriate for the composites. Moreover, the procedure used for the compliance and the contact area evaluation is also suitable.

The results concerning the composites with values of ratio E_f/E_s different from 1 are shown in Figs. 12 and 13 (Figs. (a) and (b), E_f/E_s is higher than 1 and in Figs. (c) and (d) E_f/E_s is lower than 1). In these figures, the values of E and $1/E$ are represented as a function of h/t and t/h, in agreement with formulations of Eqs. (4)–(7). Most of the results were obtained with a film thickness of 0.5 μm. However, for the cases of composites C1 and C10, results were obtained for a thickness value of 0.165 μm, allowing to conclude that the composite Young's modulus results are independent of the film's thickness, when represented as function of h/t (or t/h). The results of this study illustrate how the Young's modulus of the composite depends on the indentation depth. Moreover, it seems from the figures that the composite Young's modulus approach faster the film or the substrate Young's modulus ($E \to E_f$, when $h \to 0$ and $E \to E_s$, when $h \to \infty$) in some cases of representa-

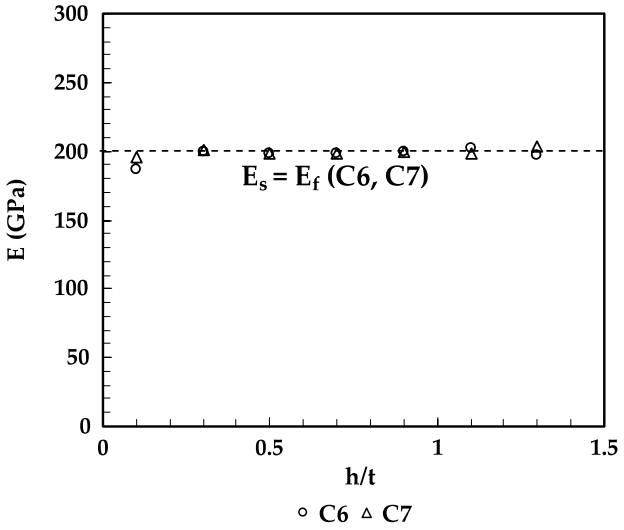

Fig. 11. Evolution of the Young's modulus versus the ratio h/t obtained for the composites with $E_f = E_s$.

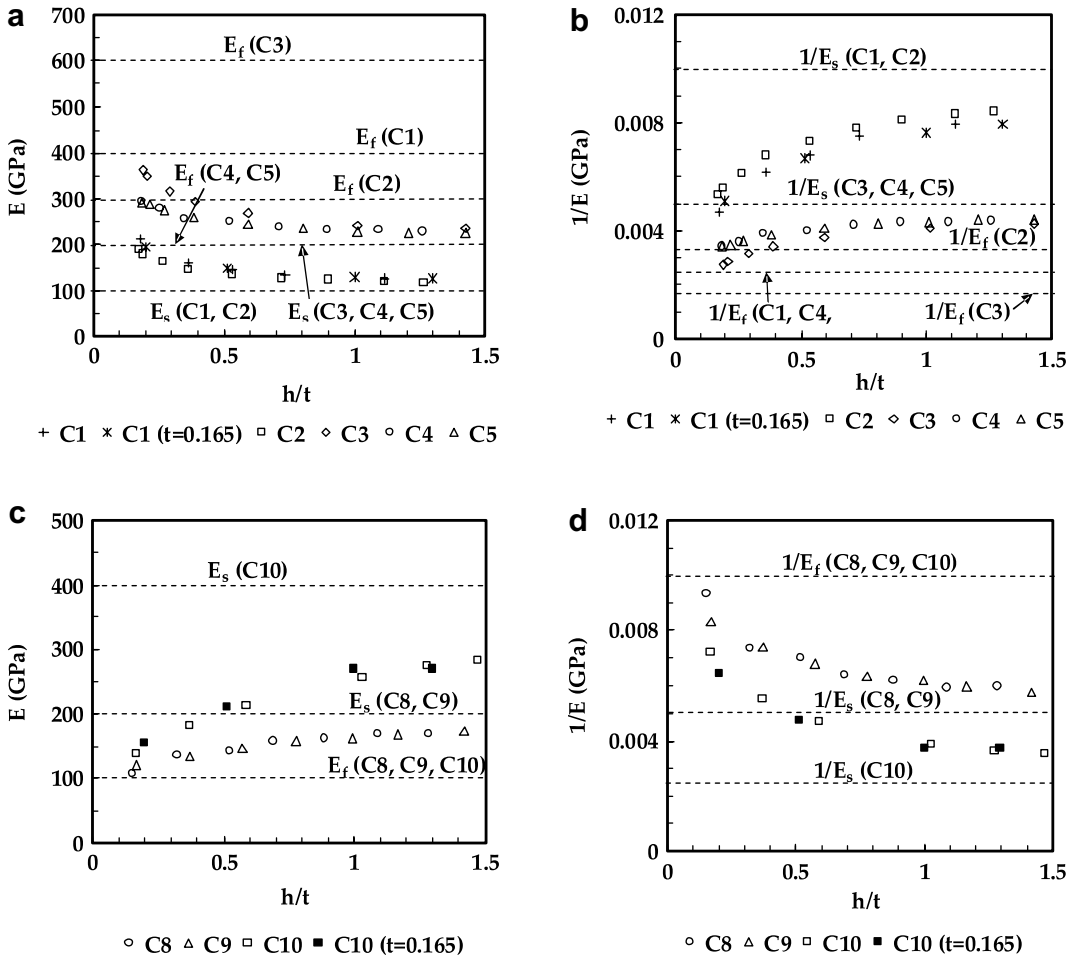

Fig. 12. Evolution of the Young's modulus (and its inverse) versus the ratio h/t. (a) and (b) $E_f > E_s$. (c) and (d) $E_f < E_s$. These results (a) and (c) were fitted by Eq. (4) and (b) and (d) by Eq. (5).

tion than in other cases, within the range of the values of h/t (or t/h) here studied. For example, compare Fig. 11(a) and (c), when $h/t \to 0$ and Fig. 13(a) and (c), when $t/h \to 0$.

In order to realize which type of exponential function for the evaluation of the Young's modulus of the film gives better results, Eqs. (4)–(7) were applied to composites C1, C2, C3, C4, C5, C8, C9 and C10, using two different approaches, in the fitting of the experimental results. The first one is the commonly used fitting procedure that takes into account the substrate's Young's modulus value as a known parameter previously determined (Menčík et al., 1997), as above described (Section 2). In the second, the values of the Young's modulus, for the substrate and the film, are both unknown and are simultaneously determined by the fitting, as described below.

Table 2 present the results obtained for the Young's moduli of the thin films with the four exponential weight functions (Eqs. (4)–(7)), taking in the fitting procedure the value of the substrate's Young's modulus as a known parameter. The results in Table 2 show that, in general, the determined values are highly inaccurate.

The Young's modulus can also be determined by fitting the same four exponential weight equations, but assuming both the Young's modulus of the substrate and the film as unknown. The fitting of the experimental data was done with the commercial software CurveExpert®, considering a generic function in the form:

$$y = a(b \pm e^{(-cx)}), \tag{11}$$

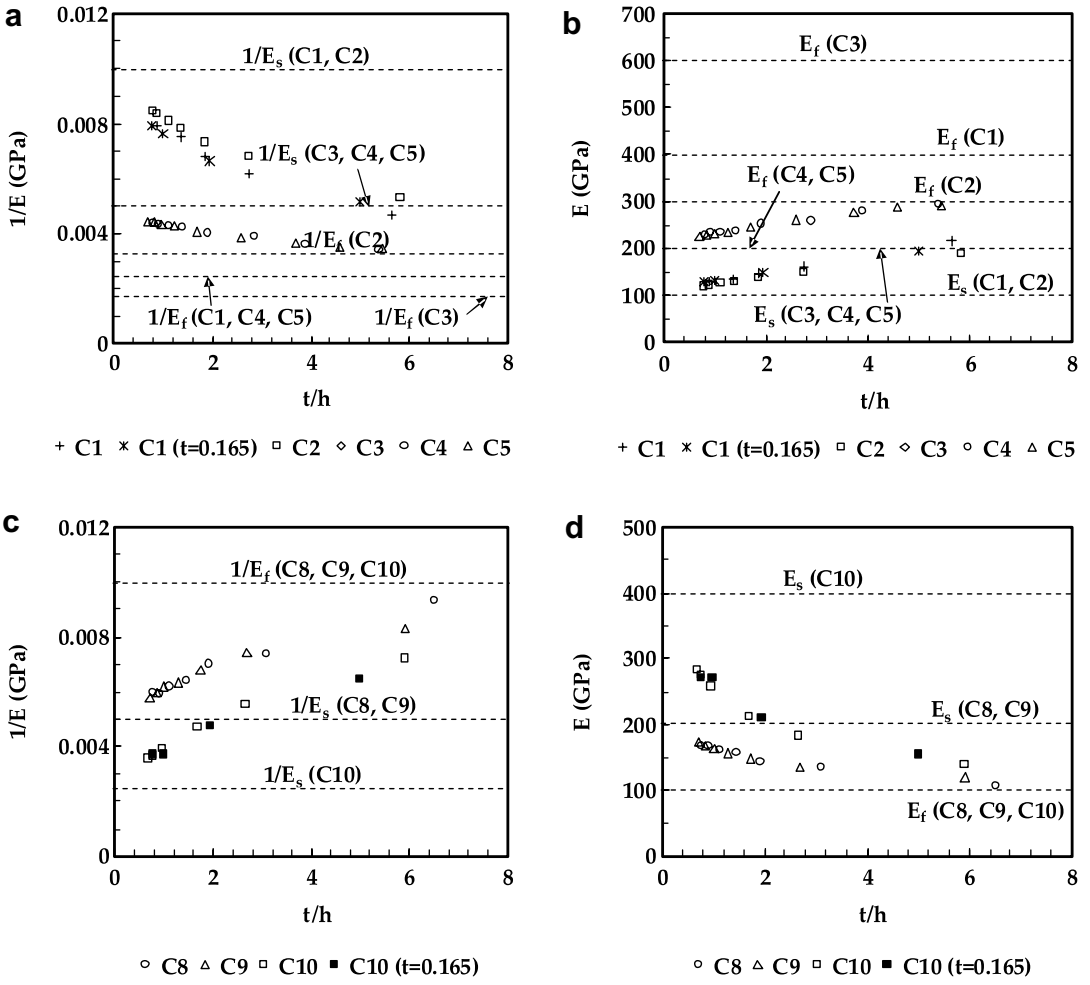

Fig. 13. Evolution of the Young's modulus and its inverse versus the ratio t/h. (a) and (b) $E_f > E_s$. (c) and (d) $E_f < E_s$. These results (a) and (c) were fitted by Eq. (6) and (b) and (d) by Eq. (7).

where y is E for the exponential functions (Eqs. (4) and (7)), or $1/E$ for the reciprocal of the exponential function and the Doerner and Nix function (Eqs. (5) and (6), respectively). x represents the ratio h/t in the case of the exponential and the reciprocal of the exponential functions (Eqs. (4) and (5)), or t/h for the Doerner and Nix functions (Eq. (6) and (7)). The constants a, b and c are obtained with the fitting procedure. Eq. (10) can be fitted to the results of the composite, using the sign (−), for: (i) $E_f < E_s$, in the case of the exponential and Doerner and Nix functions (Eqs. (4) and (6), respectively), and (ii) $E_f > E_s$ in the case of the reciprocal exponential function (Eqs. (4) and (7)). In the other cases, Eq. (11) is used with the sign (+). The meanings of the constants of Eq. (11) are: (i) for the exponential and Doerner and Nix, a is equal to $(E_s - E_f)$ if $E_f < E_s$ or $(E_f - E_s)$ if $E_f > E_s$; (ii) for the reciprocal of exponential and Eq. (7) a is equal to $(1/E_s - 1/E_f)$ if $E_f > E_s$ or $(1/E_f - 1/E_s)$ if $E_f < E_s$; (iii) the value ab is equal to E_s, E_f, $1/E_s$ and $1/E_f$ for the functions: exponential, Doerner and Nix, reciprocal of exponential and Eq. (7), respectively.

Table 3 shows the results obtained for the eight composites, where E_f/E_s is not equal to 1, considering the procedure described concerning the use of Eq. (11), i.e. both Young's moduli, of the substrate and the film, are determinate from the fitting. A first comment, from the comparison of the results presented in Tables 2 and 3 is that a better approach for the film's modulus is obtained, independently of the function used, when the substrate modulus is not fixed. This suggests that the use, in the fitting procedure, of a predetermined value for the substrate modulus have significant influence in the accuracy obtained for Young's modulus of the film. It

Table 2
Film Young's modulus results obtained with exponential, reciprocal exponential, Doerner and Nix, and Eq. (7), considering known the substrate modulus

Composites	Reference value	Exponential		Reciprocal exponential		Doerner and Nix		Eq. (7)	
	E_f (GPa)	E_f (GPa)	Error (%)	E_f (GPa)	Error (%)	E_f (GPa)	Error (%)	E_f (GPa)	Error (%)
$E_f > E_s$									
C1	400	227.7	43.1	245.6	38.6	241.9	39.5	336.7	15.8
C2	300	191.8	36.1	200.2	33.3	204.2	31.9	243.9	18.7
C3	600	372.4	37.9	388.5	35.2	396.4	33.9	338.0	43.7
C4	400	294.6	26.3	297.3	25.7	300.8	24.8	271.6	32.1
C5	400	297.5	25.6	301.9	24.5	301.9	24.5	275.6	31.1
Average			33.8		31.5		30.9		28.3
$E_f < E_s$									
C8	100	119.4	19.4	123.3	23.3	120.1	20.1	153.6	53.6
C9	100	110.9	10.9	115.1	15.1	113.7	13.7	147.4	47.4
C10	100	121.3	21.3	136.5	36.5	122.4	22.4	196.3	96.3
Average			17.2		24.9		18.7		65.8

The reference value indicate in the table is equal to input value used in the numerical simulation.

seems that the error in the value of the composite Young's modulus is disseminated into Young's moduli of the film and the substrate, when the substrate value is not fixed.

The analysis of the results in Table 3 enables us to conclude that, for the case of the composites with $E_f > E_s$ the most adequate method to determine the film's modulus seems to be the reciprocal of the exponential function (mean error of 6.1%); the error of the exponential function is higher (mean error of 15.4%), but better than the two others. For the composites with $E_f < E_s$, the best results are obtained with the exponential function (mean error of 3.8%), although the reciprocal of the exponential function also gives satisfactory results for the Young's modulus of the film (mean error of 8.3%). For the evaluation of the substrate's modulus, the Doerner and Nix and Eq. (7) functions appear appropriate, independently of the value of the ratio E_f/E_s (mean errors less than 6.8%). This means that the Young's modulus of the film is most satisfactorily evaluated by functions whose value is obtained by extrapolation to zero (E and $1/E$ versus h/t – see Figs. 1(a) and 12). Similarly, the Young's modulus of the substrate is most unsatisfactorily evaluated when its value is obtained by extrapolation to zero (E and $1/E$ versus t/h – see Figs. 1(b) and 13).

In order to test the Gao et al. (1992) function for the evaluation of the film Young's modulus Eq. (8) was applied to the composites C1, C2, C3, C4, C5, C8, C9 and C10, using the two different approaches for fitting the experimental results, as used before for the exponential functions. In the case where the substrate's Young's modulus is an unknown parameter the procedure uses the linear fit of the composite's Young's modulus E^* as a function of the result of Eq. (9), for different values of x ($= a/t$). In this case, the substrate's Young's modulus corresponds to the independent constant obtained in the linear fit: $y = A + Bx$, where $y = E^*$ and $B = E_f^* - E_s^*$ and x is the result of Eq. (9), for the different indentations depths, i.e. for different values of x ($= a/t$). Fig. 14 presents the evolution of the Young's modulus with Gao's weight function. Table 4 shows the results obtained for the thin films' Young's moduli with the Gao function (Eqs. (8) and (9)), using in the fitting procedure, the value of the substrate's Young's modulus as a known and unknown parameter. The results in Table 4 show that the results for the Young's modulus evaluation using the Gao function are not accurate enough, for both cases.

The above results concerning the use of exponential functions suggest that the type of fitting, E or $1/E$ as a function of h/t, can be important on the evaluation of the film's Young's modulus. For this reason, we have carried out the fitting of the following equation, deduced from the Gao function, changing E^*, E_f^* and E_s^* to $1/E^*, 1/E_f^*$ and $1/E_s^*$, respectively (identified as reciprocal of the Gao function):

$$\frac{\left(1/E^* - 1/E_s^*\right)}{\left(1/E_f^* - 1/E_s^*\right)} = \Phi. \tag{12}$$

Table 3
Young's modulus results for substrate and film obtained with exponential, reciprocal exponential, Doerner and Nix, and Eq. (7)

Composites	Reference value	Exponential		Reciprocal exponential		Doerner and Nix		Eq. (7)	
	E_f (GPa)	E_f (GPa)	Error (%)	E_f (GPa)	Error (%)	E_f (GPa)	Error (%)	E_f (GPa)	Error (%)
$E_f > E_s$									
C1	400	319.2	20.2	412.5	3.1	280.2	29.9	522.9	30.7
C2	300	255.3	14.9	289.2	3.6	237.0	21.0	356.8	18.9
C3	600	484.1	19.3	542.0	9.7	426.5	28.9	563.5	6.1
C4	400	365.5	8.6	384.6	3.8	345.5	13.6	472.4	18.1
C5	400	344.8	13.8	358.9	10.3	344.0	14.0	336.4	15.9
Average			15.4		6.1		21.5		17.9
$E_f < E_s$									
C8	100	103.6	3.6	111.5	11.5	120.6	20.6	125.3	25.3
C9	100	104.0	4.0	106.5	6.5	115.9	16.0	118.1	18.1
C10	100	96.3	3.7	106.9	6.9	118.7	18.7	132.8	32.8
Average			3.8		8.3		18.4		25.4
	E_s(GPa)	E_s(GPa)	Error (%)	E_s (GPa)	Error (%)	E_s (GPa)	Error (%)	E_s (GPa)	Error (%)
$E_f > E_s$									
C1	100	126.3	26.3	122.3	22.3	108.8	8.8	104.9	4.9
C2	100	119.5	19.5	116.9	16.9	106.8	6.8	102.4	2.4
C3	200	235.6	17.8	231.3	15.6	209.4	4.7	208.2	4.1
C4	200	229.5	14.7	228.3	14.1	214.1	7.0	214.9	7.4
C5	200	224.3	12.1	222.8	11.4	213.9	6.9	206.8	3.4
Average			18.1		16.1		6.8		4.4
$E_f < E_s$									
C8	200	178.1	10.9	178.4	10.8	204.7	2.4	200.0	0.0
C9	200	186.3	6.9	180.1	9.9	205.3	2.6	201.8	0.9
C10	400	315.6	21.1	287.4	28.1	395.5	1.1	355.5	11.1
Average			12.9		16.3		2.0		4.0

The reference value indicate in the table is equal to input value used in the numerical simulation.

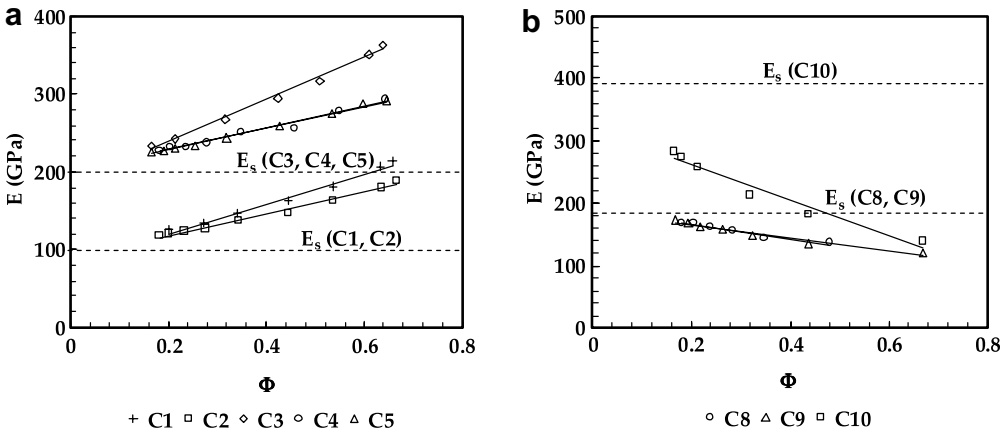

Fig. 14. Evolution of the composite Young's modulus versus the Gao's weight function, Φ. (a) $E_f > E_s$. (b) $E_f < E_s$.

In this equation, the meaning of the parameters is the same as in Eqs. (8) and (9). Also, a similar procedure to determine the Young's modulus of the film was used in the fitting of results. Fig. 15 shows the evolution of the reverse of the composite Young's modulus with the result of Gao's weight function (Eq. (9)). The comparison of Figs. 14 and 15 show that the linear behaviour is slightly better approached in the case that the reverse of the Young's modulus is used (the average of the R-squared value is 0.97 and 0.99 in Figs. 14 and 15, respec-

Table 4
Young's modulus results for substrate and film obtained with the Gao function

Composites	Reference value	Gao			
	E_f (GPa)	E_f (GPa)	Error (%)	E_f (GPa)	Error (%)
$E_f > E_s$					
C1	400	257.4	35.7	275.6	31.1
C2	300	219.3	26.9	230.3	23.2
C3	600	438.1	27.0	454.7	24.2
C4	400	340.7	14.8	339.7	15.1
C5	400	341.8	14.6	342.8	14.3
Average			23.8		21.6
$E_f < E_s$					
C8	100	58.1	41.9	71.5	28.5
C9	100	61.1	38.9	81.4	18.6
C10	100	13.6	86.4	33.2	66.8
Average			55.7		38.0
	E_s (GPa)			E_s (GPa)	Error
$E_f > E_s$					
C1	100	Equal to the input values used in the FE simulation		81.6	18.5
C2	100			90.2	9.8
C3	200			184.4	7.8
C4	200			200.8	0.4
C5	200			199.2	0.4
Average					
$E_f < E_s$					
C8	200	Equal to the input values used in the FE simulation		189.8	5.1
C9	200			186.0	7.0
C10	400			319.3	20.2
Average					10.8

The reference value indicate in the table is equal to input value used in the numerical simulation.

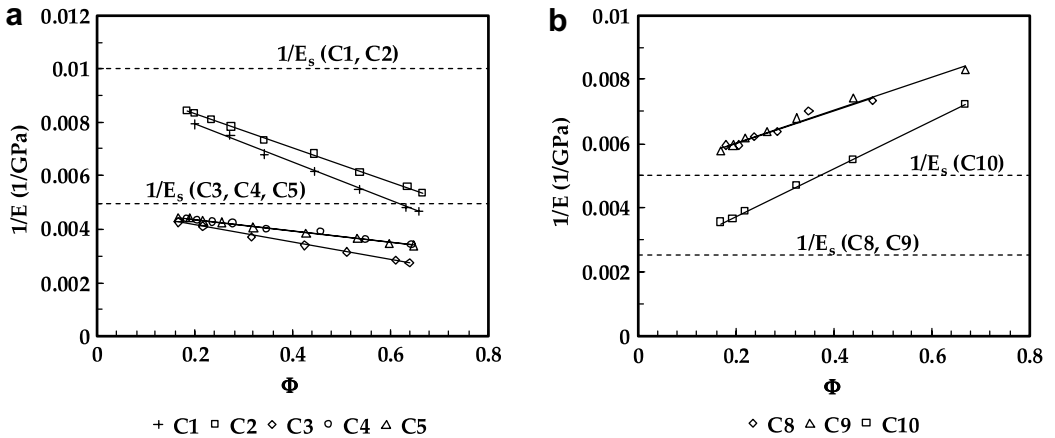

Fig. 15. Evolution of the reverse of the composite Young's modulus versus the Gao's weight function, Φ. (a) $E_f > E_s$. (b) $E_f < E_s$.

tively) The results presented in Table 5 show that Eq. (12) gives more accurate results for the Young's modulus of the film than Gao's function, independently of the procedure used (substrate, Young's modulus, known and unknown). Moreover, the most accurate results for the Young's modulus of the film are obtained using the

Table 5
Young's modulus results for substrate and film obtained with the reciprocal of Gao's function

Composites	Reference value	Reciprocal Gao			
	E_f (GPa)	E_f (GPa)	Error (%)	E_f(GPa)	Error (%)
$E_f > E_s$					
C1	400	570.5	42.6	427.0	13.5
C2	300	366.0	22.0	313.2	4.4
C3	600	735.8	22.6	628.5	4.8
C4	400	420.9	5.2	373.9	6.5
C5	400	417.9	4.5	381.9	4.3
Average			19.4		6.7
$E_f < E_s$					
C8	100	99.3	0.7	99.1	0.9
C9	100	98.6	1.4	99.0	1.0
C10	100	107.2	7.2	103.8	4.3
Average			3.1		2.1
	E_s (GPa)			E_s (GPa)	Error (%)
$E_f > E_s$					
C1	100	Equal to the input values used in the FE simulation		108.9	8.9
C2	100			104.3	4.3
C3	200			209.2	4.6
C4	200			209.5	4.8
C5	200			207.8	3.9
Average					5.3
$E_f < E_s$					
C8	200	Equal to the input values used in the FE simulation		200.3	0.2
C9	200			199.0	0.5
C10	400			440.1	10.0
Average					3.6

The reference value indicate in the table is equal to input value used in the numerical simulation.

procedure that simultaneously evaluates both Young's moduli (film and substrate). In this case, the results of the Young's modulus of the film are quite suitable for all composites independently of the ratio E_f/E_s (mean error equal to 5.4%, for the case of $E_f > E_s$, and equal to 1.9%, for the case of $E_f < E_s$). In addition, the substrate's Young's modulus is quite accurately determined (mean error equal to 5.3%, in the case where $E_f > E_s$, and equal to 3.6%, in the case where $E_f < E_s$).

In conclusion, in order to obtain accurate results for the value of the film's Young's modulus, Eqs. (4), (5) and (12) can be used for $E_f < E_s$, $E_f > E_s$ and both cases ($E_f < E_s$ and $E_f > E_s$), respectively. Moreover, the fitting of these equations to the results must be carried out taking the substrate's Young's modulus as an unknown parameter; for the cases of Eqs. (4) and (5), this can be done using Eq. (11) and the commercial software CurveExpert®. For the cases of the composites with $E_f > E_s$, the Young's modulus of the film results show a mean error of 6.7%, when obtained with the reciprocal of the Gao function (Eq. (12)), and a mean error of 6.1%, for the case of the reciprocal of the exponential function (Eq. (5)). For the composites with $E_f < E_s$, the reciprocal of the Gao (Eq. (12)) and the exponential functions also give the most suitable results for the Young's modulus of the film (mean errors of 2.1 and 3.8%, respectively). The fact that the reciprocal of the Gao function gives accurate results for the Young's moduli of film and substrate, independently of the type of composites studied ($E_f < E_s$ and $E_f > E_s$), traduces an important advantage relative to the exponential functions (Eqs. (4) and (5)), for which the accuracy depends on the ratio E_f/E_s (see Table 3).

4.2.2. Real composites

The above discussed weight functions were also applied to the experimental data of four real composite materials, in order to validate the conclusions obtained for the fictive materials with regard to the

evaluation of the films' Young's modulus. The experimental data is obtained from Menčík et al. (1997) and Saha and Nix (2002). From the study of Menčík et al. (1997), two composites that combined a TbFe + Fe film with two substrates, silicon and glass, were studied. This produces composites with $E_f < E_s$ and $E_f > E_s$ ($E_f/E_s = 0.75$ and 2.00, respectively). The remaining two composites are tungsten films on silicon and glass substrates, obtained from Saha and Nix (2002). The E_f/E_s ratios of these composites are 2.30 and 5.71, respectively. Table 6 summarizes the elastic constants of the film and substrate materials. Fig. 16 shows the evolution of the composite's Young's modulus value, E, versus the relative indentation depth, h/t (up to $h/t = 1$), for the four composites.

For the Young's modulus evaluation, the composite results in the range h/t 0.2 to 0.6 were used, as shown in Fig. 16. The choice of this range is based on the fact that for low penetration depths the indentation results can present relatively low accuracy. Besides, the maximum value of the ratio h/t must be also limited: in the case of hard films, cracking or delamination can occurs; and soft films tends to pile-up around the indenter. For both cases incorrect composite Young's modulus values can be obtained (Menčík et al., 1997). Table 7 show the results for the Young's modulus of the film obtained with the six weight functions using the fitting procedure that considers the substrate's Young's modulus as an unknown, giving the best results for all the weight functions. From Table 7, it can be concluded that the most accurate values of the Young's modulus were obtained with the reciprocal of the Gao function. In the case of the Tungsten/Glass composite, the evaluation of the Young's modulus of the film becomes significantly inaccurate for all weight functions (except the reciprocal Gao function), which may be associated with experimental inaccuracy or lack of performance of the models, probably as consequence of the high value of the ratio E_f/E_s (5.71). In conclusion, the results obtained

Table 6
Elastic constants of the real materials

Composites	Film thickness (μm)	E_f (GPa)	E_s (GPa)	ν_f	ν_s
(TbFe + Fe)/Glass (Menčík et al., 1997)	1.20	130	65	0.30	0.24
(TbFe+Fe)/Silicon (Menčík et al., 1997)	1.20	130	174	0.30	0.20
Tungsten/Glass (Saha and Nix, 2002)	0.50	410	65	0.25	0.25
Tungsten/Silicon (Saha and Nix, 2002)	0.64	410	174	0.25	0.25

Experimental data by Menčík et al. (1997) and Saha and Nix (2002).

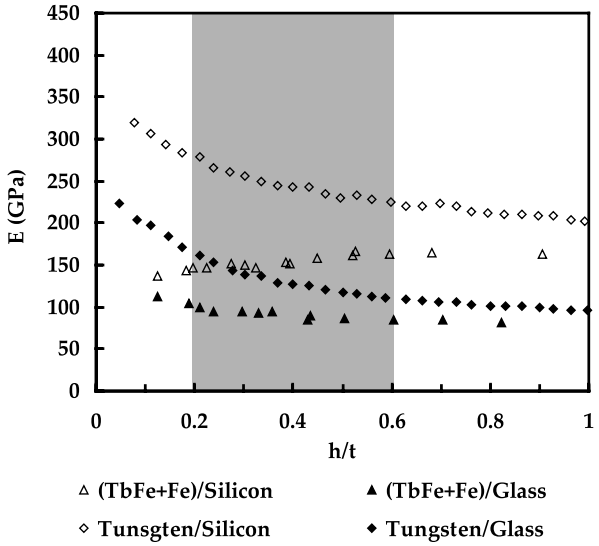

Fig. 16. Composite Young's modulus versus relative indentation depth. Experimental data by Menčík et al. (1997): composites (TbFe + Fe)/Silicon and (TbFe + Fe)/Glass. Experimental data by Saha and Nix (2002): Composites Tungsten/Silicon and Tungsten/Glass.

Table 7
Young's modulus (GPa) results of the experimental films

Composites	Exponential	Reciprocal exponential	Doerner and Nix	Eq. (7)	Gao	Reciprocal Gao
(TbFe + Fe)/Glass	107.4	102.5	92.6	98.4	111.5	130.7
Error	17.4	21.2	28.7	24.4	14.3	0.6
(TbFe + Fe)/Silicion	135.6	138.2	146.3	144.9	123.1	128.2
Error	4.3	6.3	12.6	11.5	5.3	1.4
Tungsten/Glass	245.2	219.3	188.4	233.2	225.6	425.5
Error	40.2	46.5	54.0	43.1	45.0	3.8
Tungsten/Silicon	372.2	307.3	267.6	381.8	345.7	392.2
Error	9.2	25.0	34.7	6.9	15.7	4.4

with the proposed reciprocal of the Gao function are, in all cases, clearly more accurate than with the others, confirming the results obtained with the fictive materials.

5. Conclusions

Three-dimensional numerical simulation of Vickers indentation tests were performed in order to acquire a better understanding of the mechanical behaviour of coated materials during indention. Several numerical simulations of fictitious composites with different mechanical properties of the film and the substrate were carried out, being the hardness of the film equal or higher than the substrate hardness.

The main conclusions of this study can be reported as follows:

- As previously proposed for bulk materials, the results of the composite Young's modulus obtained in the numerical simulations, for composites with the same Young's modulus, but different yield stresses for the film and the substrate, indicate that the use of a geometrical correction factor β equal to 1.05 for the Vickers indenter (Eq. (1)) enables accurate results.
- The numerical simulation results of the Vickers indentation of composites with different values of the ratio between Young's moduli of the film and substrate, gives important information about the indentation surface geometry (sink-in and pile-up formation). For the composites with ratio σ_f/σ_s equal to 1, the indentation surface geometry seems to evolve with the indentation depth from that typical of the film to that typical of the substrate, depending on the ratio between the hardness and the Young's modulus. When the ratio σ_f/σ_s is equal to 2, sink-in appears independently of the elastic properties of the film and of the substrate.
- Even for a relatively thick film (0.5 μm), the onset of elastic deformation in the substrate occurs prematurely, at a penetration depth of about 1% (or much less) of the thickness, depending on the size of the indenter offset. Moreover, at a penetration depth of about 5% of the thickness, the results obtained in numerical simulation of composites with different values of the E_f/E_s ratio indicate that significant "*errors*" can occur in the determination of the film's Young's modulus when it is considered equal to the composite Young's modulus. So, in every case, a model (weight function) must be used to evaluate the Young's modulus of thin coatings.
- The fitting of the numerical results for eight film/substrate combinations using six weight functions was performed using two different procedures. The first one, commonly used, considers the substrate's Young's modulus as a known parameter that goes into the fitting. However, for better accuracy, the fitting of these equations to the results must be carried out taking the substrate's Young's modulus as an unknown parameter. For the cases of the composites where $E_f > E_s$, the best results for the Young's modulus of the film were obtained using the reciprocal of the Gao and the reciprocal of exponential functions. For the composites where $E_f < E_s$, the reciprocal of the Gao and the exponential functions also give the most suitable results for the film's Young's modulus. These conclusions are essentially valid for both cases studied; real and fictive materials.

Acknowledgements

The authors are grateful to the Portuguese Foundation for Science and Technology (FCT) who financially supported this work, through the Program POCTI (Portuguese Government and FEDER). One of the authors, N.A. Sakharova, was supported by a grant for scientific research from the Portuguese Science and Technology Foundation. This support is gratefully acknowledged.

References

Antunes, J.M., Cavaleiro, A., Menezes, L.F., Simões, M.I., Fernandes, J.V., 2002. Ultra-microhardness testing procedure with Vickers indenter. Surface and Coatings Technology 149 (1), 27–35.

Antunes, J.M., Menezes, L.F., Fernandes, J.V., Simões, M.I., 2004. Numerical simulation of ultramicrohardness tests in thin films. Materials Science Forum, 694–698.

Antunes, J.M., Menezes, L.F., Fernandes, J.V., 2006. Three-dimensional numerical simulation of Vickers indentation tests. International Journal of Solids and Structures 43 (3–4), 784–806.

Antunes, J.M., Menezes, L.F., Fernandes, J.V., 2007. Influence of Vickers tip imperfection on depth sensing indentation tests. International Journal of Solids and Structures 44, 2732–2747.

Bhattacharya, A.K., Nix, W.D., 1988. Analysis of elastic and plastic deformation associated with indentation testing of thin films on substrates. International Journal of Solids Structures 24 (12), 1287–1298.

Bolshakov, A., Oliver, W.C., Pharr, G.M., 1997. Finite element studies of the influence of pile-up on the analysis of nanoindentation data. Materials Research Society Symposium Proceedings, vol. 436, pp. 141–146.

Burnett, P.J., Rickerby, D.S., 1987. The mechanical properties of wear-resistant coatings II: experimental studies and interpretation of hardness. Thin Solid Films 148 (1), 51–65.

Chechenin, N.G., Bottiger, J., Krog, J.P., 1995. Nanoindentation of amourphous aluminum oxide films II. Critical parameters for the breakthrough and a membrane effect in thin hard films on soft substrates. Thin Solid Films 261, 219–227.

Chen, X., Vlassak, J.J., 2001. A numerical study on the measurements of thin film mechanical properties by means of nanoindentation. Journal of Materials Research 16 (10), 2974–2982.

Doerner, M.F., Nix, W.D., 1986. A method for interpreting the data from depth-sensing indentation instruments. Journal of Materials Research 1 (4), 601–609.

Doerner, M.F., Gardner, D.S., Nix, W.D., 1986. Plastic properties of thin fims on substrates as measured by submicron indentation hardness and substrate curvature techniques. Journal of Materials Research 1 (6), 845–851.

Fabes, B.D., Oliver, W.C., McKee, R.A., Walker, F.J., 1992. The determination of film hardness from the composite response of film and substrate to nanometer scale indentations. Journal of Materials Research 7 (11), 3056–3064.

Gao, H.J., Chiu, C.H., Lee, J., 1992. Elastic contact versus indentation modeling of multi-layered Materials. International Journal of Solids Structures 29 (20), 2471–2492.

Joslin, D.L., Oliver, W.C., 1990. A new method for analyzing data from continuous depth-sensing microindentation tests. Journal of Materials Research 5 (1), 123–126.

King, R.B., 1987. Elastic analysis of some punch problems for a layered medium. International Journal of Solids and Structures 23 (12), 1657–1664.

Korsunsky, A.M., McGurk, M.R., Bull, S.J., Page, T.F., 1998. On the hardness of coated systems. Surface and Coatings Technology 99 (1), 171–183.

Menčík, J., Munz, D., Quandt, E., Weppelmann, E.R., Swain, M.V., 1997. Determination of elastic modulus of thin layers using nanoindentation. Journal of Materials Research 12 (9), 2475–2484.

Menezes, L.F., Teodosiu, C., 2000. Three-dimensional numerical simulation of the deep-drawing process using solid finite elements. Journal of Materials Processing Technology 97 (1-3), 100–106.

Oliver, W.C., Pharr, G.M., 1992. An improved technique for determining hardness and elastic modulus using load and displacement sensing indentation experiments. Journal of Materials Research 7 (6), 1564–1583.

Page, T.F., Hainsworth, S.V., 1993. Using nanoindentation techniques for the characterization of coated systems: a critique. Surface and Coatings Technology 61 (1–3), 201–208.

Pharr, G.M., Oliver, W.C., 1992. Measurement of thin-film mechanical properties using Nanoindentation. Materials Research Society Bulletin 17 (7), 28–33.

Saha, R., Nix, W.D., 2002. Effects of the substrate on the determination of thin film mechanical properties by nanoindentation. Acta Materialia 50, 23–38.

Sneddon, I.N., 1965. The relation between load and penetration in the axisymmetric Boussinesq problem for a punch of arbitrary profile. International Journal of Engineering and Science 3, 47–57.

Sun, Y., Bell, T., Zheng, S., 1995. Finite element analysis of the critical ratio of coating thickness to indentation depth for coating property measurements by nanoindentation. Thin Solid Films 258 (1–2), 198–204.

Tsui, T.Y., Vlassak, J., Nix, W.D., 1999a. Indentation plastic displacement field: Part I. The case of soft films on hard substrates. Journal of Materials Research 14 (6), 2196–2203.

Tsui, T.Y., Vlassak, J., Nix, W.D., 1999b. Indentation plastic displacement field: Part II. The case of hard films on soft substrates. Journal of Materials Research 14 (6), 2204–2209.

Tsui, T.Y., Pharr, G.M., 1999. Substrate effects on nanoindentation mechanical property measurement of soft films on hard substrates. Journal of Materials Research 14 (1), 292–301.